Strong ^{25}Al + p resonances via elastic proton scattering with a radioactive ^{25}Al beam

J. Chen,[1,*] A. A. Chen,[1] G. Amádio,[2] S. Cherubini,[3,4] H. Fujikawa,[2] S. Hayakawa,[2] J. J. He,[2,†] N. Iwasa,[5] D. Kahl,[1] L. H. Khiem,[6] S. Kubono,[2] S. Kurihara,[2] Y. K. Kwon,[7] M. La Cognata,[3] J. Y. Moon,[7] M. Niikura,[2,‡] S. Nishimura,[9] J. Pearson,[1] R. G. Pizzone,[3] T. Teranishi,[8] Y. Togano,[9] Y. Wakabayashi,[2,§] and H. Yamaguchi[2]

[1]*Department of Physics and Astronomy, McMaster University, Hamilton, Ontario L8S 4M1, Canada*
[2]*Center for Nuclear Study (CNS), University of Tokyo, Wako Branch, 2-1 Hirosawa, Wako, Saitama 351-0198, Japan*
[3]*Laboratori Nazionali del Sud-INFN, Catania, Italy*
[4]*Dipartimento di Fisica e Astronomia, Universitá di Catania, Catania, Italy*
[5]*Department of Physics, Tohoku University, 6-6 Aoba, Sendai, Miyagi 980-8578, Japan*
[6]*Institute of Physics, Vietnamese Academy for Science and Technology (VAST), 10 Daotan, Badinh, Hanoi, 10000, Vietnam*
[7]*Department of Physics, Chung-Ang University, Seoul 156-756, Republic of Korea*
[8]*Department of Physics, Kyushu University, Fukuoka 852-851, Japan*
[9]*RIKEN Nishina Center, 2-1 Hirosawa, Wako, Saitama 351-0198, Japan*

(Received 5 October 2011; revised manuscript received 31 December 2011; published 13 January 2012)

^{25}Al + p elastic scattering in inverse kinematics was measured to explore the level structure of ^{26}Si above its proton threshold. The ^{2}H(^{24}Mg, n) ^{25}Al reaction was used to produce a 3.4 MeV/nucleon ^{25}Al radioactive beam with intensities of about 10^6 ions per second on target. By using a thick target of $(CH_2)_n$, a center-of-mass energy range of 3 MeV was scanned, reaching up to about 8.5 MeV in excitation energy in ^{26}Si. This energy range covered the region of importance for the ^{25}Al(p, γ) ^{26}Si at temperatures characteristic of explosive nucleosynthesis. Level parameters of six strong s-wave ^{25}Al + p resonances in ^{26}Si were extracted from fits to the measured excitation functions using the R-matrix formalism. Two new levels have been discovered, while for two others, our spin-parity assignments disagree with the results of some previous studies. Lastly, our resonance parameters for the remaining two levels are in good agreement with past experimental work, and with recent shell-model calculations.

DOI: 10.1103/PhysRevC.85.015805 PACS number(s): 23.20.Lv, 26.30.−k, 25.40.Lw, 27.30.+t

I. INTRODUCTION

In explosive nucleosynthesis, the thermonuclear ^{25}Al(p, γ)^{26}Si ($Q_p = 5513.7(5)$ keV [1]) reaction rate plays a role in the synthesis of the γ emitter ^{26}Al^g ($t_{1/2} = 0.717$ million years), whose 1.809-MeV decay line has been a target for γ-ray astronomy [2]. The main reaction sequence leading to the synthesis of ^{26}Al^g is ^{24}Mg(p, γ)^{25}Al(β^+, ν)^{25}Mg(p, γ)^{26}Al^g. However, the ^{25}Al(p, γ)^{26}Si reaction bypasses the β^+ decay of ^{25}Al and consequently deflects the reaction flow away from ^{26}Al^g since ^{26}Si ($t_{1/2} = 2.229$ s) decays to the isomeric first-excited state in ^{26}Al, which decays in turn directly to ^{26g}Mg without emission of the 1.809-MeV γ ray (see Fig. 1).

Although classical novae are not expected to be the main source of galactic ^{26}Al (this distinction falls to massive stars [3,4]), model calculations indicate that novae may contribute at smaller but significant levels [5]. In this context, José *et al.* [5] in particular confirmed that the ^{25}Al(p, γ)^{26}Si reaction significantly affects the final ^{26}Al yield. Moreover, at the higher temperatures characteristic of shell carbon burning and explosive neon burning ($T \lesssim 2.5$ GK), the ^{25}Al(p, γ)^{26}Si reaction becomes significantly faster than the β^+ decay of ^{25}Al [6]. Under these conditions, the ground state of ^{26}Al can communicate with its isomeric first-excited state through thermal excitations, and Runkle *et al.* [7] suggested that the ^{25}Al(p, γ)^{26}Si reaction rate may be sufficiently high to produce effectively a significant amount of ^{26}Al^g through γ-ray transitions from ^{26m}Al (although see Ref. [8] for further discussion on the thermal equilibration of ^{26}Al^g and ^{26m}Al).

Apart from considerations related to galactic ^{26}Al, the ^{25}Al(p, γ)^{26}Si reaction also plays a role in type-I x-ray bursts ($T_{\text{peak}} \sim 1.5$ GK), in which the αp and rp process controls the energy generation and nucleosynthesis [9,10]. Model simulations show that ^{25}Al(p, γ)^{26}Si is activated along the rp-process paths in the burst's ignition region, following break out from the Hot Carbon-Nitrogen-Oxygen (CNO) cycles, as well as in the convective regions [9]. In a more recent study [11], the reaction was identified as one of the most important ones in the overall flow as the burst temperature approaches its peak, thus contributing strongly to the energy production. Furthermore, in the αp process, impedances in the reaction flow at selected nuclei (the "waiting points") have been shown to influence the burst's light-curve evolution [12]. In particular, the ^{25}Al(p, γ)^{26}Si reaction bridges the waiting-point nuclei ^{22}Mg and ^{26}Si through the sequence ^{22}Mg(α, p)^{25}Al(p, γ)^{26}Si(α, p)^{29}P—leading eventually to ^{30}S, a waiting point which has been implicated as a possible explanation for the existence of double-peaked bursts [12].

*chenj26@mcmaster.ca
†Present address: Institute of Modern Physics, Chinese Academy of Sciences (CAS), Nanchang Road 509, Lanzhou 730000, China.
‡Present address: Institut de Physique Nucléaire d'Orsay, IN2P3-CNRS, F-91406 Orsay Cedex, France.
§Present address: Advanced Science Research Center, Japan Atomic Energy Agency (JAEA), Naka-gun, Ibaraki 319-1195, Japan.

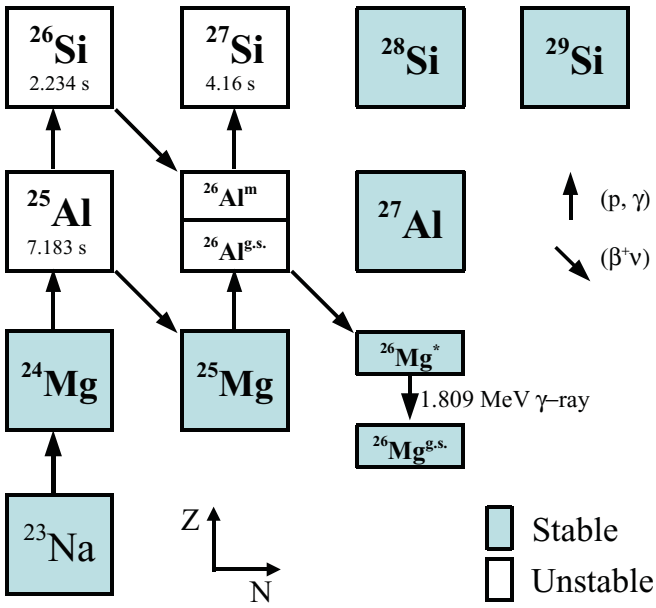

FIG. 1. (Color online) Reaction paths toward the production of the ^{26}Al. The reaction sequence producing the ^{26}Al$^{g.s.}$ is dominant at typical peak temperatures of novae ($T = 0.1$–0.4 GK), while at $T > 0.4$ GK, the one producing the ^{26}Al isomer becomes dominant. Note that ^{26}Si decays to the isomeric first-excited state in ^{26}Al, which decays directly to ^{26g}Mg without emission of the 1.809-MeV γ ray.

Since a direct measurement of the ^{25}Al$(p,\gamma)^{26}$Si reaction is unfeasible due to insufficiently intense beams of ^{25}Al, indirect approaches (e.g., transfer reactions and in-beam γ-ray spectroscopy) have been widely adopted to determine the required level properties of ^{26}Si, such as resonance energies and spin-parity assignments [6,13–22]. To complement these studies, state-of-the-art shell model calculations have recently been performed to determine theoretically those level parameters that have remained inaccessible to experiment [23]. In the most recent experimental work on the structure of ^{26}Si [6], a comprehensive evaluation of the reaction rate was carried out, in which contributions from ^{25}Al $+ p$ resonances with energies up to $E_R \sim 2.6$ MeV [or $E_x(^{26}\text{Si}) \sim 8$ MeV] were included.

While the contributions from low-lying resonances [$E_x(^{26}\text{Si}) \lesssim 6$ MeV] to the ^{25}Al$(p,\gamma)^{26}$Si rate at nova temperatures have been largely determined or at least significantly constrained, at the higher temperatures, s-wave resonances with $E_x(^{26}\text{Si}) \sim 6$–$8$ MeV will also contribute to the reaction rate. Although some states in this energy region have been discovered (see the level compilation in Ref. [6]), many of their level parameters remain unmeasured. Moreover, a comparison between the relevant energy regions in ^{26}Siand ^{26}Mg reveals missing states in the former, some of which could be ^{25}Al $+ p$ s-wave resonances and thus potentially important for the ^{25}Al$(p,\gamma)^{26}$Si rate.

In light of the above, further study of the structure of ^{26}Si by other reaction mechanisms is warranted. Resonant proton scattering in particular has been demonstrated to be sensitive to broad s-wave resonances (e.g., Refs. [24–26]). To that end, we have performed for the first time a study of ^{25}Al $+ p$ resonances in ^{26}Si using proton elastic scattering, with the aim of better characterizing known states that may be important to the stellar ^{25}Al$(p,\gamma)^{26}$Si reaction rate, while searching for new states as well.

II. EXPERIMENT

The experiment was performed in inverse kinematics at the Center for Nuclear Study (CNS) Radioactive Ion Beam (CRIB) separator [27], owned and operated by the University of Tokyo and located on the RIKEN campus in Wako, Japan. The primary beam of ^{24}Mg^{8+} was accelerated to 7.5 MeV/nucleon by the Azimuthally Varying Field (AVF) cyclotron and impinged on a cooled ^{2}H gas target. The secondary beam of radioactive ^{25}Al ($t_{1/2} = 7.183$ s) was produced via the ^{2}H(^{24}Mg, n)^{25}Al reaction and separated with a pair of magnetic dipoles. Further separation through a velocity separator (Wien filter) resulted in a beam energy of about 3.4 MeV/nucleon, a purity of about 50%, and an intensity of up to 1.2×10^6 pps on the secondary target. The ^{25}Al beam ions were identified and separated from the remaining ^{24}Mg contaminants with two parallel plate avalanche counters (PPACs) [28] located just upstream from the secondary target. These PPACs were also used for beam tracking to determine the beam position on the secondary target and the scattering angle.

The secondary target was a 6.58 m/cm^2 polyethylene $(CH_2)_n$ foil, which was thick enough to stop the heavy beam ions, thus allowing the thick-target method [29,30] for measuring resonant proton scattering to be used. This technique has been used successfully in several earlier experiments at CRIB (e.g., Refs. [26,31,32]). Along the path of the beam particle, from the front of the $(CH_2)_n$ target to its stopping location, the beam particle continuously loses energy mainly due to collisions with electrons in the target, and scatters the light target particles into forward angles in the laboratory system. Therefore, a wide range of ^{26}Si excitation energy can be scanned simultaneously with only one beam energy. For our target thickness, a center-of-mass energy range of $\sim$3 MeV was scanned, reaching up to about 8.5 MeV in excitation energy in ^{26}Si.

The elastically scattered protons were detected downstream from the target by three sets of ΔE-E telescopes centered at laboratory angles of 0°, 17°, and 27°, all having the same distance of 204 mm from the target center and the same angular opening of about 14°. Each telescope consisted of one 75 μm double-sided position-sensitive silicon detector (PSD), with 16×16 strips and an area of 5×5 cm^2, and two 1500 μm single-channel silicon strip detectors (SSDs).

To identify the scattered protons, a two-dimensional histogram of their energy losses (ΔE) in a PSD versus their total energies (E) was used for the protons that punched through the PSD, while for those stopping in the PSD, a histogram of ΔE versus the time-of-flight (TOF) between the second PPAC and the PSD was used. Figure 2 shows the particle identification for the former case.

The silicon detectors (PSDs and SSDs) were first calibrated separately with standard alpha sources. A further calibration of the silicon telescopes with proton beams with energies of 5, 9, and 14 MeV was used to correct for the pulse-height

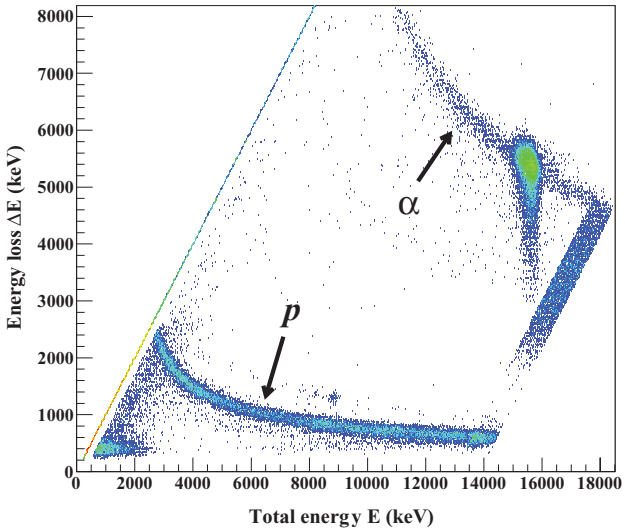

FIG. 2. (Color online) Two-dimensional histogram of ΔE (energy loss) vs E (total energy), on which was performed the particle identification of protons that punched through the position-sensitive silicon detectors (PSDs). To obtain this histogram, a gate on the ^{25}Al beam ions was applied on the time-of-flight between the radio frequency (rf) signal from the AVF cyclotron and the PPAC.

defect due to different detector responses to alpha particles and protons [33]. Since in our experiment the detector energy thicknesses for protons is about 3 MeV for the PSD and about 16 MeV for the SSD, the calibration protons punched through the PSDs but stopped in the SSDs, enabling the entire ΔE-E telescope to be calibrated.

Lastly, directly above the target, an array of ten NaI detectors was used to detect γ rays from the decay of the first-excited state of the ^{25}Al, in an attempt to determine the contribution from inelastic proton scattering by measuring the deexcitation γ rays. However, it was very difficult to determine the contribution from this channel mostly due to the large background of γ rays. In particular, no clear evidence for the 452 keV transition from the first-excited state of ^{25}Al to its ground state was observed. It was also found that the γ-proton coincidence yield is very small compared to the total yield. Therefore, in the analysis it was assumed that the elastic scattering channel is dominant.

III. DATA ANALYSIS AND RESULTS

A. Energy-loss corrections for scattered protons

From conservation of momentum and kinetic energy, the conversion between the total kinetic energy in the center-of-mass frame ($E_{\mathrm{c.m.}}$) and the measured energy of the scattered protons in the laboratory frame (E_p) for the elastic scattering in inverse kinematics is given by

$$E_{\mathrm{c.m.}} = \frac{M+m}{4M\cos^2\theta_{\mathrm{lab}}} E_p, \qquad (1)$$

where M and m are the nuclear masses of the heavy beam particle and the scattered proton, respectively, and θ_{lab} is the scattering angle between the proton's scattering direction and the beam direction. For thin targets, the energy loss of the reaction products in the target is small and therefore can be safely neglected compared to their exit energies. However, when using the thick-target technique, the energy loss of the scattered proton traveling through the remaining part of the target can be considerable and must be taken into account.

In our analysis, this energy-loss correction was effected an event-by-event basis as follows: The range of the ^{25}Al beam ion in the $(CH_2)_n$target was determined (see below) and divided into 5000 equal segments. Starting from the front end of the target, the residual energy of the ^{25}Al beam was calculated in each segment with standard energy-loss routines [34]. The energy of the scattered proton at the scattering location was also calculated. For a given path length of the proton through the target, its energy after the target was determined and compared with the measured proton energy in a single event. This process was iterated with an optimization algorithm until the calculated energy matched the measured one. The on-spot proton energy of this event (i.e, the energy of the proton corrected for the energy loss) was thus directly deduced from the best match of the comparison procedure.

In order to determine the range of the ^{25}Al beam ions in the target, the angle at which the beam particle enters the target (with respect to the horizontal direction) must be calculated. This angle, along with the position of the beam ion on the target, was obtained from the track of the beam particle as determined by the two PPACs located upstream of the target. The proton detection position in the PSD in turn gave the angle at which the proton leaves the target. The scattering angle θ_{lab} is thus simply the angle between this beam ion track and the recoil proton's track.

B. Dead-layer effect and background subtraction

Each of the silicon detectors used in the experiment has a dead layer of 2-μm-thick aluminum deposited on top of the silicon content. Since the dead layer does not contribute to the detector's charge collection, there will be an energy loss in the layer that will be unaccounted for in the determination of the total energy deposited. As a consequence of this effect, a gap within which no events are counted appears in the proton energy spectrum for the energy range corresponding to that of the protons that stop in the dead layer. With the beam energy of 3.4 MeV/nucleon used in this experiment, no protons from ^{25}Al + p resonant scattering are energetic enough to punch through the first SSD detector. Therefore, the only gap is caused by the two dead layers between the PSD (ΔE) and the first SSD (E), corresponding to a small energy range ($\sim$100 keV) around $E_{\mathrm{c.m.}} = 0.8$ MeV.

Since a $(CH_2)_n$ target was used in this experiment, most of the background in the proton energy spectrum came from reactions on the carbon in the target. To subtract this background, measurements were carried out with a pure carbon target, under identical conditions to those of the production run. The proton yield from the pure carbon target was then normalized to the yield from the carbon in the $(CH_2)_n$ target based on the total accumulated number of beam

events, the carbon number densities of the two targets, and the energy-dependent stopping powers of the ^{25}Al beam in the $(CH_2)_n$ and C foils. The normalization factor of the yield from pure carbon to the yield from carbon in $(CH_2)_n$ was calculated as follows:

To calculate the normalization factor, we chose a beam-energy step-size δE_b equal to the bin size ($\delta E_{\text{c.m.}}$) of the proton spectrum in the center-of-mass frame. The target thickness traversed by the beam corresponding to any energy bin in the proton spectrum is thus given by $\delta x = \delta E_b/S$, where $S = dE/dx$ is the energy-dependent stopping power of the beam in the target material. The yield in the thick-target technique in any energy bin can then be calculated from

$$Y = I\sigma n\delta x = I\sigma n\frac{\delta E_b}{S}, \tag{2}$$

where I is the total accumulated number of beam events, σ is the cross section of the reaction of the beam ions with carbon nuclei, and n is the number density of the carbon in the respective target.

Hence, the normalization factor N is determined from

$$N = \frac{Y_1}{Y_2} = \frac{I_1}{I_2}\frac{n_1}{n_2}\Big/\frac{S_1}{S_2}, \tag{3}$$

where I_1 and I_2 are the total accumulated number of ^{25}Al beam ions bombarding the $(CH_2)_n$ and carbon targets, respectively, and assumed to be constant over the whole path traveled by the beam ions, n_1 is the equivalent number density of carbon in the $(CH_2)_n$ target, n_2 is the same number density in the pure carbon foil, and S_1 and S_2 are the corresponding stopping powers of the beam ions in the two targets. This normalization factor is then applied to the yield in each bin of the proton spectrum from the runs with the pure carbon target, which is then subtracted from that of the production runs with the $(CH_2)_n$ target. This subtraction was performed after adjusting the two spectra to have the same bin size (energy per bin). Figure 3 shows the proton spectra from these two targets as well as the final spectrum after energy-loss corrections and background subtraction, and with the proton energies converted from the laboratory frame to the center-of-mass frame.

C. Experimental cross section and *R*-matrix analysis

The experimental differential cross sections in the laboratory frame were calculated from the yield [Eq. (2)] and the solid angle $\delta\Omega$ covered by the detector and is given by

$$\frac{d\sigma}{d\Omega_{\text{lab}}} = \frac{YS}{In\delta E_{\text{c.m.}}\delta\Omega}\frac{m}{M+m}, \tag{4}$$

where $\delta E_{\text{c.m.}} = \frac{m}{m+M}\delta E_b$ is the conversion between the beam energy E_b and the center-of-mass energy $E_{\text{c.m.}}$, and $\delta\Omega \sim 0.05$ sr for all three detector angles in this experiment.

Since the integrals of the differential cross sections over the same solid angle in the laboratory frame and the center-of-mass frame are equal, that is,

$$\frac{d\sigma}{d\Omega_{\text{lab}}}d\Omega_{\text{lab}} = \frac{d\sigma}{d\Omega_{\text{c.m.}}}d\Omega_{\text{c.m.}}, \tag{5}$$

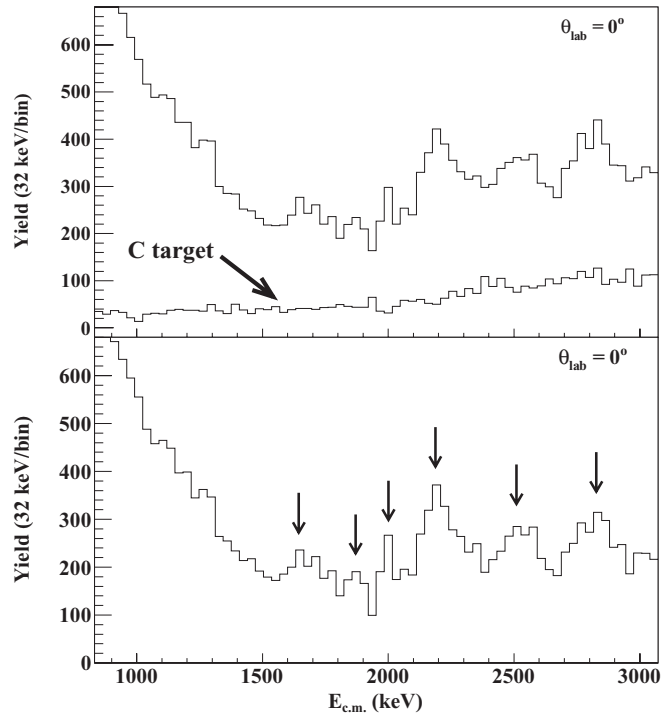

FIG. 3. Top: energy-loss-corrected proton spectra from the $(CH_2)_n$ target and the pure carbon target. Bottom: proton spectrum after energy-loss correction and background subtraction. Some potential resonance structures are indicated with arrows. The energy axis is chosen to start right after the region corresponding to the dead layer of the silicon detectors (see text for discussion).

and since the relation between the scattering angles in the two frames is $2\theta_{\text{lab}} + \theta_{\text{c.m.}} = 180^\circ$, where θ_{lab} and $\theta_{\text{c.m.}}$ are the scattering angles in the laboratory frame and the center-of-mass frame, respectively, we calculated the differential cross sections in the center-of-mass frame from the proton yield shown in Fig. 3 using

$$\frac{d\sigma}{d\Omega_{\text{c.m.}}} = \frac{1}{4\cos\theta_{\text{lab}}}\frac{YS}{In\delta E_{\text{c.m.}}\delta\Omega}\frac{m}{M+m}, \tag{6}$$

and fit the resulting excitation functions using the R-matrix formalism. The uncertainty in the cross sections includes systematic and statistical contributions (the latter are dominant, while the former are mainly from the target and detector geometry, as well as the accumulated beam ion counts).

The general multichannel multilevel R-matrix formula for the differential cross section of any resonant process from an entrance channel α to an exit channel α' is given by [35,36],

$$\frac{d\sigma_{\alpha\alpha'}}{d\Omega_{\alpha'}} = \frac{1}{(2J_1+1)(2J_2+1)}\sum_{ss'}(2s+1)\frac{d\sigma_{\alpha s,\alpha' s'}}{d\Omega_{\alpha'}}, \tag{7}$$

where J_1 and J_2 are the spins of the nuclei in the entrance channel; α and α' symbolize the entrance and exit channels; s and s' are the channel spins of the entrance and the exit channels; and the summation is over all of the partial differential cross sections of different combinations of channel spins s and s'. The partial differential cross section can be

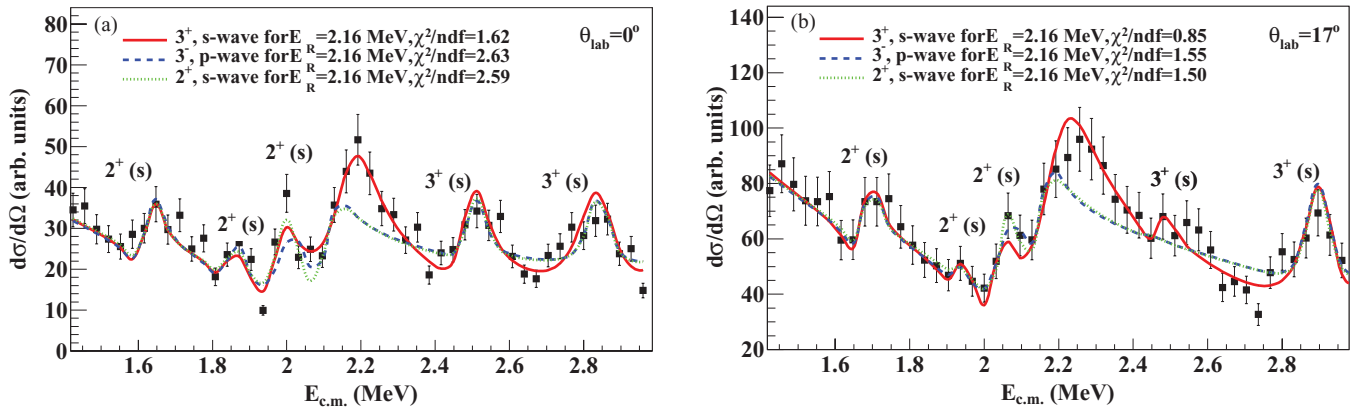

FIG. 4. (Color online) Excitation functions of elastically scattered protons at laboratory angles of (a) $\theta_{\rm lab} = 0^\circ$ and (b) $\theta_{\rm lab} = 17^\circ$, showing R-matrix fits for six resonances between $E_R = 1.4$ and 2.9 MeV. In both panels, the solid line is the best fit with s-wave ($l = 0$) scattering and $J^\pi = 2^+$, 2^+,2^+, 3^+, 3^+, and 3^+; the dashed and dotted lines are fits with the J^π of the $E_R = 2.16$ MeV resonance changed to 3^- and 2^+, respectively.

written as

$$\frac{d\sigma_{\alpha s,\alpha' s'}}{d\Omega_{\alpha'}} = \frac{\pi}{(2s+1)k_\alpha^2}(CT + RT + IT), \tag{8}$$

where k_α is the wave number and CT, RT, and IT represent the three components of the resonant differential cross section—the Coulomb term, resonant term, and interference term, respectively [35].

The CT and IT terms are nonzero when the entrance channel and exit channel are identical (i.e., in elastic scattering). In our experiment, we take the open channel to be elastic scattering, and since the s-wave contribution is dominant for low-energy scattering, an orbital momentum transfer of $l = 0$ is also assumed. Under these assumptions, the multichannel multilevel R-matrix formula is thus reduced to a single-channel formalism [25].

The RT and IT terms are determined from an energy dependent R-matrix element, R_l, which contains the physics information and is given for our simplified case by

$$R = \sum_\lambda \frac{\gamma^2}{E_\lambda - E}, \tag{9}$$

where γ and E_λ are the reduced width and pole energy of a resonance, respectively, which are thus the two resonance parameters to be extracted from the fit to the data. From these, the physical resonance energy E_R and width Γ_R can in turn be obtained after a proper boundary transformation [37–40]. The R-matrix fitting was performed using the same code used and described in Refs. [25,41]. Input parameters required for the fitting procedure include the reaction channel radius [$r_c = 1.2(A_1^{1/3} + A_2^{1/3})$], initial pole energies and reduced widths, and the spins and parities assigned to the resonances to be fit. For each combination of input parameters, the best fit was found, in convolution with the experimental resolution. The spin and parity of a given resonance were determined by the fit with the smallest χ^2 of all these best fits. The fit was found to be insensitive to changes in the channel radius. The resonance energy and width are directly extracted from the fit and the boundary transformation procedure.

The possible combinations of the nuclear quantum numbers are derived from conservation of total angular momentum before and after the scattering. The ground state of ^{25}Al has spin-parity J^π of $\frac{5}{2}^+$ and the proton has $\frac{1}{2}^+$, which couple together to give channel spin $S = \frac{5}{2} \oplus \frac{1}{2} = 2$ or 3. The spin parity of the compound nucleus is determined by $J = l \oplus S$ and $\pi_f = \pi_i \pi_p (-1)^l$, where l is the relative orbital quantum number of the proton with respect to the heavy reacting nucleus; and π_i, π_f, and π_p represent the parities of the initial heavy reacting nucleus, the final compound nucleus, and the proton, respectively.

Since at low energies ($E_R \lesssim 1.2$ MeV) Coulomb scattering is dominant, no unambiguous resonance signature was observed in the excitation function over this energy region (the widths of the resonances in this region are also expected to be too narrow). In the highest energy region covered in our measurement ($E_R \gtrsim 2.9$ MeV), some indications of resonance-like structures were observed, but these were not statistically significant and could not be properly fit. However, six resonances were identified in the energy range from 1.4 to 2.9 MeV. This corresponds to a ^{26}Si excitation energy range of about 6.9 to 8.4 MeV.

The excitation functions were fit with different spin-parity combinations for the six resonances and the best fit was determined, as shown in Fig. 4(a). (For the excitation function from $\theta_{\rm lab} = 27^\circ$, the resonances structures were not discernible and therefore this data set was not fit.) Table I lists the

TABLE I. Resonance energies and widths for six resonances in the energy range of about 1400–2900 keV, from the best R-matrix fit. The uncertainties quoted are statistical ones from the fit.

E_λ(MeV)	E_R(MeV)	Γ_R(keV)
1.670(14)	1.648(14)	7(4)
1.897(40)	1.888(40)	6(4)
2.027(13)	1.970(13)	46(11)
2.242(13)	2.190(13)	41(6)
2.518(14)	2.501(14)	15(5)
2.860(12)	2.842(12)	27(8)

TABLE II. Level energies (MeV) and spin-parities in ^{26}Si in the range of 7.1 to 8.3 MeV from present work in comparison with those of previous studies (see text for discussion). An adopted value of $S_p = 5513.5(5)$ keV was used to deduce the level energies from proton resonance energies. The uncertainties quoted in the present work are statistical ones from the R-matrix fits (a systematic uncertainty of 20 keV should be added).

This work	(p,t) [20][a]	(p,t) [6]	(p,t) [13][a]	β^+ decay [16][d]	(^{3}He, n) [15][b]	(^{4}He,^{6}He) [19]	(^{3}He, n) [21][a]	(p,t) [22][a]
7.162(14), 2^+	7.157(4), 2^+	7.151(5)	7.160(5)		7.152(4), 2^+	7.161(6)	7.150(30), 2^+	7.150(15)
7.402(40), 2^+	7.439(6), (2^+)	7.4152(23), (4^+)[a]	7.425(7), (2^+)		7.425(4), 0^+	7.429(7)	7.390(30), (0^+)	
7.484(13), 2^+	7.512(8), (2^+)	7.479(12)	7.498(4)	7.501(5), 2^+	7.493(4), 2^+	7.480(20)	7.480(30), 2^+	7.476(20)
				7.606(6)				
		7.522(12), (5^-)[c]						
	7.672(2), 3^-	7.661(12), (2^+)[c]	7.687(22), 3^-		7.694(4), 3^-	7.676(4)		7.695(31)
7.704(13), 3^+		7.701(12)						
	7.875(2), 1^-	7.874(4)	7.900(22), 1^-		7.899(4), 1^-	7.885(4)	7.900(30)	7.902(21)
				7.962(5)				
8.015(14), 3^+								
				8.156(21), 2^+			8.120(30), (2^+)	
		8.222(5), (1^-)[c]						
		8.269(4), (2^+)[c]		8.254(5)				
8.356(12), 3^+								

[a] J^π from a Distorted-Wave-Born-Approximation (DWBA) analysis.
[b] J^π from a Hauser-Feshbach analysis.
[c] J^π from a mirror assignment.
[d] J^π from allowed β^+ decay and comparisons with shell-model calculations.

resonance parameters for the six resonances extracted from the R-matrix fit. The listed uncertainties in these parameters are statistical from the fit. For the resonance energies, a systematic uncertainty of 20 keV should be included, which is mainly due to uncertainties in the aforementioned calibration of the detectors using proton beams. The corresponding level energies and spin-parities in comparison with those from previous studies are given in Table II, with the adopted value of $S_p = 5513.5(5)$ keV determined from a weighted average of recent results (i.e., 5513.2(29) keV [42], 5513.7(5) keV [1] and 5512.3(11) keV [43]).

IV. DISCUSSIONS AND CONCLUSIONS

The best fits to the six resonances were for s-wave scattering, as shown in Fig. 4(a) and in Table I. No good fits were achieved with p-wave ($l = 1$) or higher-l transfer values to any of the six resonances, and hence all the levels are assigned positive parity. For the states at $E_x = 7.162$ and 7.484 MeV, all good fits give $J^\pi = 2^+$, which, together with the level energies, are in good agreement with all previously reported assignments for these two levels from transfer reaction studies [6,13,15,20]. Furthermore, a recent shell-model calculation [23] also predicted these two states to have proton widths comparable to the experimental values determined from our work.

For the second resonance, corresponding to $E_x = 7.402$ MeV, our $J^\pi = 2^+$ assignment agrees with the tentative 2^+ assignments of Bardayan *et al.* [13] and Chipps *et al.* [20], but disagrees with the measured value of 0^+ from Parpottas *et al.* [15]. This situation is further complicated by the indication in Ref. [20] that the peak observed in their work is a doublet, and by the fact that the poor statistics in our experiment results in a relatively large uncertainty in this level's resonance energy.

The fourth resonance is best fit with a $J^\pi = 3^+$ assignment. While fits with $J^\pi = 2^+$ and 3^- can be marginally achieved [see Fig. 4(a)], the fit for $J^\pi = 3^+$ gives a significantly better χ^2 value than those of the other two assignments. Our excitation energy for this state is $E_x = 7.704$ MeV. Prior to the most recent studies by Chipps *et al.* [20] and Matic *et al.* [6], the states observed by Paddock [22], Bardayan *et al.* [13], and Parpottas *et al.* [15], at $E_x = 7.695(31)$, 7.687(22), and 7.694(4) MeV, respectively, were identified as the same state based on the $J^\pi = 3^-$ assignment determined in the last two of these studies. However, in the more recent study of Chipps *et al.* [20], which used the same reaction as Bardayan *et al.* [13] but with an improved energy calibration, this $J^\pi = 3^-$ state was measured at $E_x = 7.672(2)$ MeV instead. Furthermore, in the recent high-resolution study of Matic *et al.* [6], also with an improved calibration relative to earlier work, *two* states in this region were measured at $E_x = 7.661(12)$ and 7.701(12) MeV (but without firm spin-parity assignments), suggesting that the first of these states should be identified with the 7.672(2)-MeV, 3^- state observed by Chipps *et al.* [20]. While the energy of the 7.694(4)-MeV, 3^- state seen by Parpottas *et al.* [15] agrees with the second of the two states from Matic *et al.* [6], a comparison between the energies of Refs. [6,15] for states with $E_x \gtrsim 7.4$ MeV shows that the energies of the latter are systematically higher than those of the former by about 10–15 keV. Thus, one possible consistent picture, as suggested in Table II, is that our state could be identified with the 7.701-MeV state of Ref. [6] with an assignment of $J^\pi = 3^+$, while the other aforementioned studies observed the $J^\pi = 3^-$ state. Further experiments are required to clarify this issue. The fifth resonance corresponds to a level at 8.015 MeV, which has not been observed before. This resonance can be fit well with both $J^\pi = 3^+$ and 2^+, but better with the former. Two levels in ^{26}Mg—one at 8.251 MeV with $J^\pi = 3^+$ and another at 8.399 MeV with unknown spin-parity assignment—could be

candidate mirror levels for this state, based on the possible mirror assignments proposed by Matic *et al.* [6].

Our sixth resonance at $E_R = 2.842$ MeV can be fit well only with $J^\pi = 3^+$. The corresponding ^{26}Si level lies at 8.356 MeV and has also not been observed before. This new level may have as a mirror partner in ^{26}Mg the 8.670-MeV level with $J = (3, 5)$ [44].

Lastly, our excitation functions also indicate that there could be one additional weak resonance around $E_R = 2.80$ MeV as seen in Fig. 4(a). Based on its level energy, it would correspond most probably to the level at $E_x = 8.269$ MeV in the work of Matic *et al.* [6]. However, the possibility of its being a fluctuation cannot be ruled out due to the large error bars. Thus, it was excluded from the present R-matrix analysis.

In summary, the structure of proton-unbound states of ^{26}Si states has been studied using resonant proton scattering and a radioactive beam of ^{25}Al, produced with the in-flight approach. Using the thick-target technique, six s-wave resonances were identified up to $E_{\text{c.m.}} \sim 2.9$ MeV, corresponding to $E_x(^{26}\text{Si}) \sim 8.3$ MeV. Their excitation energies and spin-parity assignments were extracted using the R-matrix formalism. Two of the levels have resonance parameters that agree well with those of previously observed states and recent shell-model calculations. For two of our states, however, our spin-parity assignments are in disagreement with some previous measurements. Lastly, two new levels corresponding to ^{25}Al + p s-wave resonances have been discovered.

While these states are expected to affect the thermonuclear ^{25}Al$(p, \gamma)^{26}$Si reaction rate at the highest temperatures found in explosive nucleosynthesis, we postpone a full evaluation of ^{25}Al$(p,\gamma)^{26}$Si rate until ongoing γ-ray spectroscopy work on ^{26}Si states—which may have implications for the lower temperatures found in nova nucleosynthesis—are completed (see, e.g., Refs. [45,46]).

ACKNOWLEDGMENTS

We are grateful to the staff members of the RIKEN accelerator group, the CRIB maintenance group, and the CNS ion source group for the high-quality radioactive beam. This work was supported by the Natural Sciences and Engineering Research Council of Canada (NSERC), and by KAKENHI (Japan) under Grant No. 21340053. A. A. C. was also funded by an Ontario Premier's Research Excellence Award (PREA) and by the DFG cluster of excellence "Origin and Structure of the Universe."

[1] T. Eronen *et al.*, Phys. Rev. C **79**, 032802 (2009).
[2] R. Diehl *et al.*, Astron. Astrophys. **298**, 445 (1995).
[3] J. Knödlseder, Astrophys. J. **510**, 915 (1999).
[4] R. Diehl *et al.*, Nature (London) **439**, 45 (2006).
[5] J. José, A. Coc, and M. Hernanz, Astrophys. J. **520**, 347 (1999).
[6] A. Matic *et al.*, Phys. Rev. C **82**, 025807 (2010).
[7] R. Runkle, A. E. Champagne, and J. Engel, Astrophys. J. **556**, 970 (2001).
[8] C. Iliadis, A. E. Champagne, A. Chieffi, and M. Limongi, Astrophys. J. Suppl. Ser. **193**, 16 (2011).
[9] J. L. Fisker, H. Schatz, and F.-K. Thielemann, Astrophys. J. Suppl. Ser. **174**, 261 (2008).
[10] A. Parikh, J. José, F. Moreno, and C. Iliadis, Astrophys. J. Suppl. Ser. **178**, 110 (2008).
[11] J. José, F. Moreno, A. Parikh, and C. Iliadis, Astrophys. J. Suppl. Ser. **189**, 204 (2010).
[12] J. L. Fisker, F.-K. Thielemann, and M. Wiescher, Astrophys. J. **608**, L61 (2004).
[13] D. W. Bardayan *et al.*, Phys. Rev. C **65**, 032801 (2002).
[14] J. A. Caggiano *et al.*, Phys. Rev. C **65**, 055801 (2002).
[15] Y. Parpottas *et al.*, Phys. Rev. C **70**, 065805 (2004).
[16] J.-C. Thomas *et al.*, Eur. Phys. J. A **21**, 419 (2004).
[17] D. W. Bardayan *et al.*, Phys. Rev. C **74**, 045804 (2006).
[18] D. Seweryniak *et al.*, Phys. Rev. C **75**, 062801 (2007).
[19] Y. K. Kwon *et al.*, J. Korean Phys. Soc. **53**, 1141 (2008).
[20] K. A. Chipps *et al.*, Phys. Rev. C **82**, 045803 (2010).
[21] W. Bohne *et al.*, Nucl. Phys. A **378**, 525 (1982).
[22] R. A. Paddock, Phys. Rev. C **5**, 485 (1972).
[23] W. A. Richter, B. A. Brown, A. Signoracci, and M. Wiescher, Phys. Rev. C **83**, 065803 (2011).
[24] D. W. Bardayan *et al.*, Phys. Rev. Lett. **83**, 45 (1999).
[25] C. Ruiz *et al.*, Phys. Rev. C **71**, 025802 (2005).
[26] J. J. He *et al.*, Phys. Rev. C **76**, 055802 (2007).
[27] S. Kubono *et al.*, Eur. Phys. J. A **13**, 217 (2002).
[28] H. Kumagai *et al.*, Nucl. Instrum. Methods Phys. Res., Sect. A **470**, 562 (2001).
[29] K. P. Artemov *et al.*, Yad. Fiz. **52**, 634 (1990).
[30] S. Kubono, Nuc. Phys. A **693**, 221 (2001).
[31] T. Teranishi *et al.*, Phys. Lett. B **650**, 129 (2007).
[32] J. J. He *et al.*, Phys. Rev. C **80**, 015801 (2009).
[33] T. R. King *et al.*, Nucl. Instrum. Methods **88**, 17 (1970).
[34] J. F. Ziegler, *The Stopping and Ranges of Ions in Matter* (Pergamon Press, Oxford, 1980), Vol. III, IV.
[35] A. M. Lane and R. G. Thomas, Rev. Mod. Phys. **30**, 257 (1958).
[36] E. Vogt, Rev. Mod. Phys. **34**, 723 (1962).
[37] F. C. Barker, Aust. J. Phys. **24**, 777 (1971).
[38] F. C. Barker, Aust. J. Phys. **25**, 341 (1972).
[39] C. Angulo and P. Descouvemont, Phys. Rev. C **61**, 064611 (2000).
[40] C. R. Brune, Phys. Rev. C **66**, 044611 (2002).
[41] E. C. Simpson, Master's thesis, University of Surrey, 2006 (unpublished).
[42] A. A. Kwiatkowski *et al.*, Phys. Rev. C **81**, 058501 (2010).
[43] A. Parikh, J. A. Caggiano, C. Deibel, J. P. Greene, R. Lewis, P. D. Parker, and C. Wrede, Phys. Rev. C **71**, 055804 (2005).
[44] The ENSDF Database, [http://www.nndc.bnl.gov/ensdf/].
[45] J. Chen *et al.* (unpublished).
[46] T. Komatsubara *et al.* (unpublished).